

Peptide backbone-copper ring structure:A molecular insight into copper-induced amyloid toxicity

Jing Wang(王静), Hua Li(李华), Xiankai Jiang(姜先凯), Bin Wu(吴斌), Jun Guo(郭俊), Xiurong Su(苏秀榕), Xingfei Zhou(周星飞), Yu Wang(王宇), Geng Wang(王耿), Heping Geng(耿和平), Zheng Jiang(姜政), Fang Huang(黄方), Gang Chen(陈刚)§, Chunlei Wang(王春雷), Haiping Fang(方海平), and Chenqi Xu(许琛琦)

Citation: Chin. Phys. B, 2022, 31 (**10**): 108702. DOI: 10.1088/1674-1056/ac8920
Journal homepage: http://cpb.iphy.ac.cn; http://iopscience.iop.org/cpb

What follows is a list of articles you may be interested in

Molecular dynamics simulations of A-DNA in bivalent metal ions salt solution

Jingjing Xue(薛晶晶), Xinpeng Li(李新朋), Rongri Tan(谈荣日), and Wenjun Zong(宗文军)
Chin. Phys. B, 2022, 31 (**4**): 048702. DOI: 10.1088/1674-1056/ac3caa

Tunable inhibition of *β*-amyloid peptides by fast green molecules

Tiantian Yang(杨甜甜), Tianxiang Yu(俞天翔), Wenhui Zhao(赵文辉), and Dongdong Lin(林冬冬)
Chin. Phys. B, 2021, 30 (**8**): 088701. DOI: 10.1088/1674-1056/ac0690

Effect of interaction between loop bases and ions on stability of G-quadruplex DNA

Han-Zhen Qiao(乔汉真), Yuan-Yan Wu(吴园燕), Yusong Tu(涂育松), and Cong-Min Ji(祭聪敏)
Chin. Phys. B, 2021, 30 (**1**): 018702. DOI: 10.1088/1674-1056/abb7f7

Structural and dynamical mechanisms of a naturally occurring variant of the human prion protein in preventing prion conversion

Yiming Tang(唐一鸣), Yifei Yao(姚逸飞), and Guanghong Wei(韦广红)†
Chin. Phys. B, 2020, 29 (**10**): 108710. DOI: 10.1088/1674-1056/aba9ba

Electron beam irradiation on novel coronavirus (COVID-19): A Monte-Carlo simulation

Guobao Feng(封国宝), Lu Liu(刘璐), Wanzhao Cui(崔万照), Fang Wang(王芳)
Chin. Phys. B, 2020, 29 (**4**): 048703. DOI: 10.1088/1674-1056/ab7dac

---

RAPID COMMUNICATION

Peptide backbone-copper ring structure: A molecular insight into copper-induced amyloid toxicity

Jing Wang(王静)[1,†], Hua Li(李华)[2,†], Xiankai Jiang(姜先凯)[3,†,‡], Bin Wu(吴斌)[2], Jun Guo(郭俊)[2], Xiurong Su(苏秀榕)[1], Xingfei Zhou(周星飞)[1], Yu Wang(王宇)[4], Geng Wang(王耿)[4], Heping Geng(耿和平)[4], Zheng Jiang(姜政)[4], Fang Huang(黄方)[5], Gang Chen(陈刚)[4,6,§], Chunlei Wang(王春雷)[7], Haiping Fang(方海平)[8], and Chenqi Xu(许琛琦)[2,9,¶]

[1] *Faculty of Science, Ningbo University, Ningbo* 315211, *China*
[2] *National Center for Protein Science Shanghai, State Key Laboratory of Molecular Biology, Institute of Biochemistry and Cell Biology, Shanghai Institutes for Biological Sciences, Chinese Academy of Sciences, Shanghai* 200031, *China*
[3] *School of Sciences, Changzhou Institute of Technology, Changzhou*, 213032, *China*
[4] *Shanghai Synchrotron Radiation Facility, Shanghai Institute of Applied Physics, Chinese Academy of Sciences, Shanghai* 201800, *China*
[5] *Center for Bioengineering and Biotechnology, China University of Petroleum (Huadong), Qingdao* 266580, *China*
[6] *School of Physical Science and Technology, ShanghaiTech University, Shanghai* 200031, *China*
[7] *Shanghai Advanced Research Institute, Chinese Academy of Sciences, Shanghai* 201210, *China*
[8] *School of Physics and National Engineering Research Center of Industrial Wastewater Detoxication and Resource Recovery, East China University of Science and Technology, Shanghai* 200031, *China*
[9] *School of Life Science and Technology, ShanghaiTech University, Shanghai* 200031, *China*

(Received 2 July 2022; revised manuscript received 3 August 2022; accepted manuscript online 12 August 2022)

Copper ions can promote amyloid diseases that are associated with amyloid peptides, such as type 2 diabetes (T2D), Alzheimer's disease (AD), Parkinson's disease (PD), and amyotrophic lateral sclerosis (ALS). However, the underlying molecular mechanism remains obscure. Here we present that Cu^{2+} is able to specifically bind to the backbone of T2D-related human islet amyloid polypeptide (hIAPP) by forming a ring structure, which causes the reduction of Cu^{2+} to Cu^{+} to produce reactive oxygen species (ROS) and the modulation of hIAPP aggregation. Nuclear magnetic resonance spectroscopy showed that Cu^{2+} bound to the backbone of a turn region, His18–Ser21, which is critical for hIAPP aggregation. *Ab initio* calculations and x-ray absorption fine structure analyses revealed that Cu^{2+} simultaneously bound with both the amide nitrogen and carbonyl oxygen on the peptide backbone, resulting in a ring structure, and causing the reduction of Cu^{2+} to Cu^{+} to form a hIAPP-Cu^{+} complex. 2′,7′-dichlorodihydrofluorescin diacetate fluorescence measurements further indicated that this complex led to enhanced ROS levels in rat insulinoma cells. Additionally, thioflavin T fluorescence and atomic force microscopy measurements denoted that the backbone-Cu ring structure largely modulated hIAPP aggregation, including the inhibition of hIAPP fibrillation and the promotion of peptide oligomerization. These findings shed new light on the molecular mechanism of Cu^{2+}-induced amyloid toxicity involving both the enhancement of ROS and the modulation of hIAPP aggregation.

Keywords: interactions between metal ion and protein, quantum chemistry calculation, protein aggregation, amyloid diseases

PACS: 87.15.–v, 87.15.kp, 31.15.ae, 68.37.Ps **DOI:** 10.1088/1674-1056/ac8920

1. Introduction

Copper ions are closely associated with amyloid diseases, such as type 2 diabetes (T2D), Alzheimer's disease (AD), Parkinson's disease (PD), and amyotrophic lateral sclerosis (ALS).[1–7] Clinical findings showed that the Cu concentrations of T2D and AD patients were significantly higher than that of healthy people.[8,9] However, the mechanism of Cu^{2+}-mediated amyloid toxicity remains obscure.[7,10] There are two prevailing views, the oxidative stress hypothesis and the oligomer hypothesis, for amyloid toxicity. In the first hypothesis, oxidative stress was suggested as a major player in the pathogenesis of amyloid diseases. The binding of redox-active Cu^{2+} to the amyloid peptide can induce the donation of electrons from amyloid peptide to Cu^{2+} ion to form a peptide-Cu^{+} complex, which can stimulate oxidative stress in a toxicity manner.[11–13] In the second hypothesis, oligomers or oligomer-like structures, rather than fibrils, were proposed to be the major cause of amyloid diseases.[14,15] Cu^{2+} can promote the oligomerization of T2D-related human islet amyloid polypeptide (hIAPP) and inhibit the fibrillation of these peptides.[16,17] Under certain conditions, Cu^{2+} and small molecules can also promote the oligomerization of AD-

†These authors contributed equally to this work.
‡Corresponding author. E-mail: jiangxk@czu.cn
§Corresponding author. E-mail: gchen@shanghaitech.edu.cn
¶Corresponding author. E-mail: cqxu@sibcb.ac.cn

© 2022 Chinese Physical Society and IOP Publishing Ltd

related amyloid-β peptides (Aβ) in a concentration-dependent manner.[18–21] These different views highlight the importance of elucidating the interaction mode of Cu^{2+} with amyloid peptides at the atomic level, which can largely promote the understanding of copper-induced amyloid toxicity.

Here, based on various biophysical approaches and theoretical analyses, we investigated the interaction of Cu^{2+} with hIAPP (Protein Data Bank (PDB) code 2KB8), which is a typical amyloid peptide that is implicated in T2D.[22] We revealed that Cu^{2+} can specifically bind to the backbone of hIAPP by forming a ring structure, causing the reduction of Cu^{2+} to Cu^{+} to produce reactive oxygen species, the inhibition of hIAPP fibrillation and the promotion of peptide oligomerization.

2. Results and discussion

2.1. Backbone-Cu ring structure of hIAPP peptide

We first performed nuclear magnetic resonance (NMR) spectroscopy to explore the specific binding sites of Cu^{2+} in the hIAPP(11-28) peptide, which is a fragment involved in amyloid aggregation.[23] Titrating with Cu^{2+} caused specific signal reduction of the cross peaks between Hβ and the backbone amide protons of His18, Ser19, Ser20 and Ser28, as well as the cross peak between Hα and the backbone amide proton of Ser28 (Fig. 1). In contrast, Zn^{2+} did not induce reductions in specific signals of the hIAPP peptide (Fig. 1). These results strongly suggest that Cu^{2+}, but not Zn^{2+}, is able to specifically bind to the backbones of His18, Ser19 and Ser20. In addition to the backbones of His18−Ser20, peak intensity changes of sidechains were also detected. The intensities of the cross peak between the imidazole Hδ2 and Hβ of His18 and the cross peak between the carboxamide NH21 and NH22 of Asn21 were specifically reduced upon Cu^{2+} titration (supplementary Figs. 1 and 2, Table 1). In contrast, the intensities of these cross peaks remained nearly unchanged with Zn^{2+} addition.

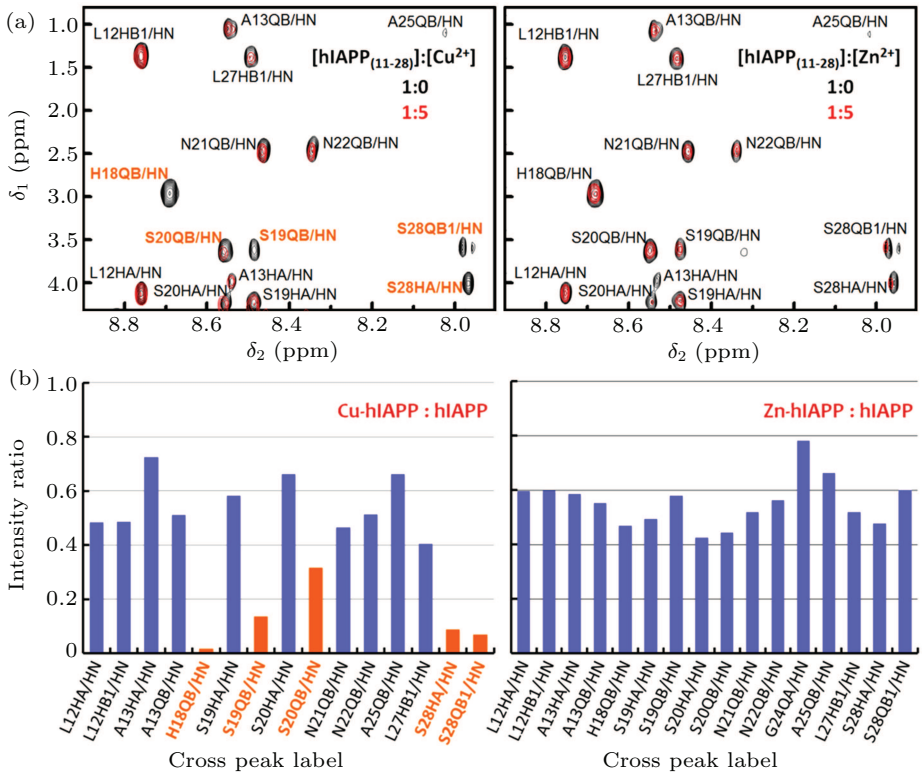


Fig. 1. Specific binding of Cu^{2+} to the backbone of hIAPP. (a) Superimposed ^{1}H–^{1}H TOCSY spectra of the hIAPP(11-28) peptide in the region of the backbone amide groups. Left: with (red) and without (black) the addition of Cu^{2+}. Right: with (red) and without (black) Zn^{2+}. The orange labels indicate the cross peaks exhibiting a substantial change caused by the addition of metal ions. (b) Cross peak intensity changes in hIAPP(11-28) caused by Cu^{2+} and Zn^{2+}. The intensity ratio between with and without the addition of Cu^{2+} (left) or Zn^{2+} (right) based on ^{1}H–^{1}H TOCSY spectra in the region of the hIAPP backbone amide groups. The orange denotes the cross peaks with an intensity ratio of less than 0.32.

Based on the NMR observations and considering the potential match between the size of the Cu^{2+} ion and the space between the neighboring amide nitrogen and carbonyl oxygen atoms of the peptide backbone, we proposed that Cu^{2+} may bind to the hIAPP backbone by forming a ring structure (Fig. 2(a)). A model peptide, HCO-Ser-NH_2, was used together with a hydrated Cu^{2+} ion ($[Cu(H_2O)_5]^{2+}$)[24] (denoted as $Cu(aq)^{2+}$) to simulate the interaction of Cu^{2+} with the Ser19 or Ser20 backbone in hIAPP. As shown by *ab initio* simulations, $Cu(aq)^{2+}$ can strongly interact simultaneously with a carbonyl oxygen (–O–) and its neighboring amide nitrogen (–N–) in the backbone, thereby resulting in a ring structure composed of Cu, –N–, –O– and the neighboring carbonyl carbon C1 and α-carbon C2 in the peptide backbone (Fig. 2(a) right),

which is denoted as –O–Cu(aq)–N–. The binding energy of this state was calculated to be −27.65 kcal/mol (Fig. 2(c), Eq. (1)), which was much stronger than the thermal fluctuation (approximately 0.6 kcal/mol at $T = 300$ K) and the hydrogen bond strength (approximately 5.0 kcal/mol) of water. This result strongly suggests that $Cu(aq)^{2+}$ is stably bound to the backbone –O– and –N–, whereas the two water molecules initially coordinated to Cu^{2+} are released, and the amide hydrogen H initially bound to –N– is substituted by Cu^{2+} (Fig. 2(a), right). In the structure –O–Cu(aq)–N–, the distances of Cu to the nearest neighboring atoms –N– and –O– and to the next nearest neighboring atoms C1 and C2 were 1.87 Å, 1.96 Å, 2.70 Å and 2.81 Å, respectively. The Cu–O distance (1.96 Å) in –O–Cu(aq)–N– was less than the averaged distance (2.03 Å) of Cu–O in $[Cu(H_2O)_5]^{2+}$. Subsequent occupied orbital analyses of –O–Cu(aq)–N– showed that few electrons were present that simultaneously belonged to the Cu, –N– and –O–, suggesting weak covalent bonds of the Cu with the –N– and –O– atoms. Moreover, the Cu ion bound to the peptide backbone exhibited a Mullikan charge of only $+0.94e$, indicating that Cu^{2+} is reduced to Cu^{+} to form a peptide-Cu^{+} complex. Additionally, the backbone-Cu ring structure –O–Cu(aq)–N– was also found in the simulations of $Cu(aq)^{2+}$ binding to the backbone of peptide model HCO-His-NH_2 for His18.

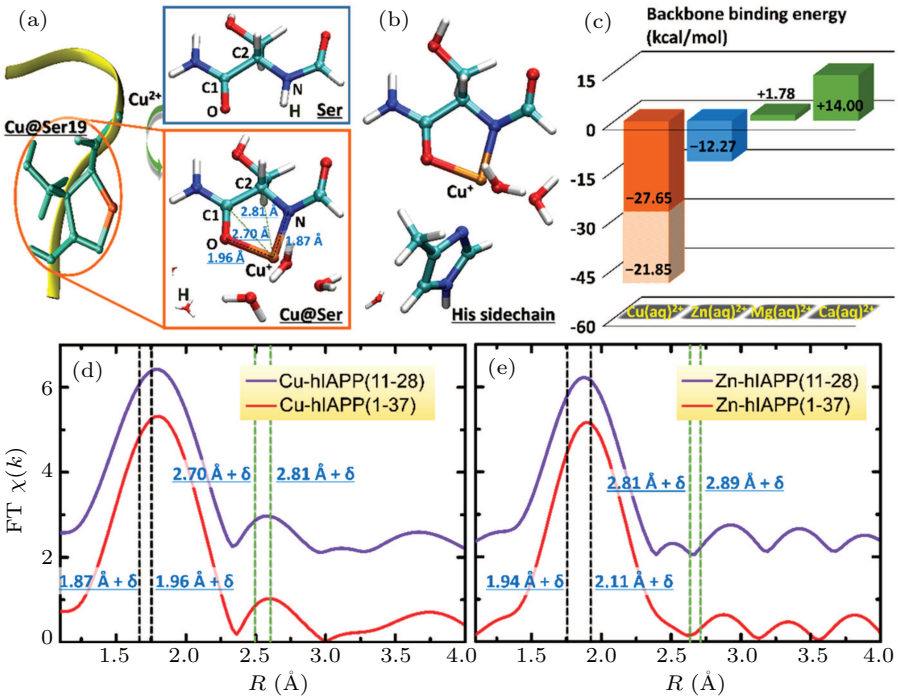


Fig. 2. Formation of backbone-Cu ring structure upon the binding of Cu^{2+} to hIAPP. (a)–(c) A theoretical model of Cu^{2+} binding to the hIAPP backbone by forming a ring structure. (a) Upon Cu^{2+} binding to the Ser backbone, the amide hydrogen H (in the upper panel, right) is substituted by Cu^{2+} (in the lower panel, right), and Cu^{2+} is reduced to Cu^{+}. Left: The yellow ribbon, light green sticks and brown sphere stand for hIAPP backbone, Ser19 and Cu ion, respectively. Right: The model peptide HCO-Ser-NH_2. The cyan, blue, red, white and brown spheres represent carbon, nitrogen, oxygen, hydrogen and copper, respectively. The labels, N, H, O, C1 and C2, indicate the amide nitrogen, amide hydrogen, carbonyl oxygen, carbonyl carbon and α-carbon of the peptide backbone, respectively. The black and green dashed lines indicate the distances of Cu to the nearest neighboring and the next nearest neighboring atoms, respectively. (b) The assistance of His sidechain to the backbone-Cu^{2+} binding. (c) Binding energies of the hydrated ions $Cu(aq)^{2+}$, $Zn(aq)^{2+}$, $Mg(aq)^{2+}$ and $Ca(aq)^{2+}$ with the peptide backbone, calculated by *ab initio* approaches. In the absence of the His sidechain, the binding strength of $Cu(aq)^{2+}$ (orange column) is much stronger than that of $Zn(aq)^{2+}$ (blue column). Green columns present that $Mg(aq)^{2+}$ and $Ca(aq)^{2+}$ cannot bind to the peptide backbone. The His sidechain can further stabilize the backbone-Cu^{2+} binding by providing additional binding energy (light orange column). (d)–(e) The Fourier-transformed EXAFS spectra (FT $\chi(k)$) of the M^{2+} ions (M = Cu or Zn) in the hIAPP(11-28) (violet) and hIAPP(1-37) (red) solutions to study the distance of the M ions to their neighboring atoms upon their binding to hIAPP. The two black and two green vertical dashed lines indicate the theoretical distances of the M to the nearest neighboring atoms N and O and to the next nearest neighboring atoms C1 and C2, respectively, in the backbone-M ring structure with a shift of $\delta = -0.23$ Å for M = Cu, and $\delta = -0.22$ Å for M = Zn. The shift δ is estimated by taking the difference between EXAFS spectra and the theoretical results of the M–O distance in the hydrated M^{2+} ion (supplementary Fig. 4).

For comparison, we also simulated the interaction of the peptide backbone with other physiological divalent cations such as Zn^{2+}, Mg^{2+} and Ca^{2+}. We calculated the binding energies of $[Zn(H_2O)_6]^{2+}$,[25] $[Mg(H_2O)_6]^{2+}$ and $[Ca(H_2O)_6]^{2+}$ with the Ser backbone using the conditions identical to those applied for $[Cu(H_2O)_5]^{2+}$. The binding energy of $Zn(aq)^{2+}$ in this state was −12.27 kcal/mol, which was much weaker than the binding energy (−27.65 kcal/mol) of $Cu(aq)^{2+}$ in the ring structure (Fig. 2(c)), indicating that a potential backbone ring structure of Zn^{2+} is substantially less stable than that of the Cu ion. The binding energies of $Mg(aq)^{2+}$ and $Ca(aq)^{2+}$ were +1.78 kcal/mol and +14.00 kcal/mol (Fig. 2(c), green columns), respectively. The positive values indicate that Mg^{2+} and Ca^{2+} cannot bind to the peptide backbone to form a ring

structure. The specific backbone-Cu^{2+} binding behavior may be attributed to the ability of Cu^{2+}, but not Zn^{2+}, Mg^{2+} and Ca^{2+}, to accept an electron and be reduced to a monovalent cation. Additional simulations suggested that the His18 sidechain can enhance the stability of the backbone-Cu binding. *Ab initio* calculations showed that the Cu^{+} ion in the ring structure –O–Cu(aq)–N– can further bind to a nitrogen in the His sidechain (Fig. 2(b)), whereas one water molecule initially coordinated to Cu^{+} was displaced. The calculated binding energy of the –O–Cu(aq)–N– structure with the His sidechain (Eq. (2)) reached −21.85 kcal/mol (Fig. 2(c), light orange column), which enhanced the peptide binding strength of Cu^{2+} to −49.50 kcal/mol. The stability of the backbone-Cu ring structure thus can be further enforced by the assistance of the His sidechain. Notably, the Mullikan charge of Cu coordinated with only the His sidechain was calculated to be $+1.39e$, indicating that, in the absence of binding to the peptide backbone, His sidechain binding alone is insufficient to reduce Cu^{2+} to Cu^{+}.

We then used x-ray absorption fine structure (XAFS) spectroscopy to confirm the presence of the backbone-Cu ring structure. The extended x-ray absorption fine structure (EXAFS) spectrum in real space (Fig. 2(d)) of Cu^{2+} in the hIAPP(11-28) solution was highly similar to that in the hIAPP(1-37) solution, indicating that hIAPP(11-28) represents the major region of hIAPP(1-37) that binds Cu^{2+} ions (more details in supplementary Fig. 3). In both spectra, the first peak was observed at 1.80 Å, which may be related to the calculated Cu–N (1.87 Å) and Cu–O (1.96 Å) distances in the backbone-Cu ring structure and the Cu–O distance (2.03 Å) in $Cu(aq)^{2+}$, via a shift of $\delta = -0.23$ Å. The shift δ was estimated by taking the difference between EXAFS spectra and theoretical results of the Cu–O distance in the first solvation shell of the hydrated Cu^{2+} ion (supplementary Fig. 4). Importantly, the second peak at 2.58 Å was consistent well with the calculated Cu–C1 (2.70 Å) and Cu–C2 (2.81 Å) distances in the ring structure via this shift δ. Moreover, our previous x-ray absorption near edge structure (XANES) analysis (Fig. 3(a)) further confirmed that Cu^{2+} could be reduced to Cu^{+} upon binding hIAPP, resulting in an hIAPP-Cu^{+} complex.[26] The major peak of the spectrum for Cu in the hIAPP(1-37) solution was clearly observed at the same location as the peak of Cu^{2+} in the $CuCl_2$ solution (8995.7 eV), suggesting that most of the copper ions in the hIAPP solution stay in solution. Interestingly, a shoulder peak appeared in the left region of the major peak. To present the location of this minor peak clearly and exactly, the derivative was performed over the spectrum, and a zero value corresponding to the shoulder peak was clearly observed at 8983.0 eV, which was very close to the location 8982.1 eV of Cu^{+} in the Cu_2O solution, indicating the presence of cuprous ions in the sample, following by the formation of the hIAPP-Cu complex. This result agreed well with the theoretical observation that Cu^{2+} was reduced to Cu^{+} upon binding the peptide backbone. Therefore, these XAFS analyses strongly support the notion of the backbone-Cu^{+} ring structure of hIAPP. A ring structure was also observed upon Al ions binding to phosphoglycerate kinase protein.[27] In contrast, the XAFS spectra (EXAFS in Fig. 2(e) and XANES in supplementary Fig. 5) of Zn^{2+} suggest that Zn^{2+} cannot bind to the backbone of hIAPP, and then cannot be reduced in hIAPP solution (seeing the detailed discussion in supplementary information).

3. Peptide backbone-Cu ring structure and the enhancement of reactive oxygen species

Given that the reduction of Cu^{2+} to Cu^{+} can lead to the generation of reactive oxygen species (ROS),[11–13] we studied the potential effect of Cu^{2+} binding to the peptide backbone on intracellular redox homeostasis. We used a molecular probe 2′,7′-dichlorodihydrofluorescin diacetate (DCFH-DA) to detect oxidative stress in rat insulinoma cells (INS-1). The fluorescence intensity of the probe was proportional to the ROS amount.[28] When INS-1 cells were incubated with

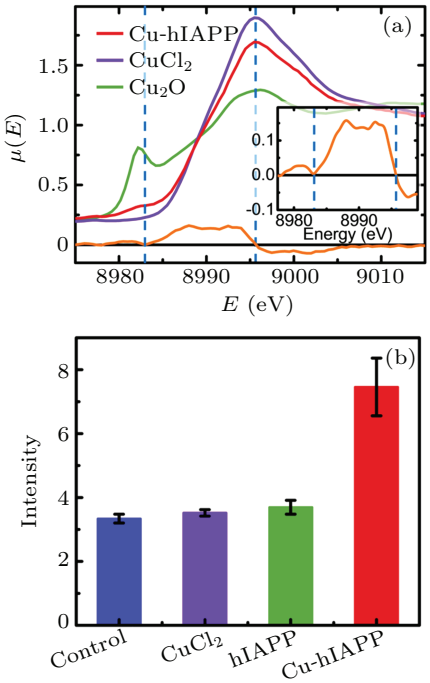


Fig. 3. Reduction of Cu^{2+} to Cu^{+} upon binding to hIAPP peptide and the enhancement of ROS level in rat insulinoma cells (INS-1) induced by the hIAPP-Cu^{+} complex. (a) XANES spectra of the Cu ion in hIAPP(1-37) solution. The red, violet and green curves represent the spectra of the Cu ion in the hIAPP solution, Cu^{2+} and Cu^{+} ions in aqueous solution, respectively. The blue dashed lines indicate the location of the major and shoulder peaks of the red curve. The orange curve represents the derivative of the Cu-hIAPP spectrum, and a detailed view of the Cu-hIAPP derivative spectrum is presented in the inset. (b) The blue, violet, green and red columns indicate the DCFH-DA fluorescence intensities of the control, the INS-1 cells incubated with $CuCl_2$, hIAPP(1-37) and hIAPP(1-37)-Cu^{+} complex, respectively. The fluorescence intensity is proportional to the intracellular ROS level.[28]

20 μM hIAPP(1-37) or 100 μM Cu^{2+} alone, the fluorescence intensities (Fig. 3(b)) were comparable to that of control (untreated) cells, indicating that hIAPP or Cu^{2+} alone cannot induce the increase of ROS in the cells. Interestingly, when INS-1 cells were incubated with both hIAPP(1-37) and Cu^{2+}, the fluorescence intensity was significantly stronger than that of the control, denoting that the presence of both hIAPP and Cu^{2+} induced a significant increase in the intracellular ROS level. These results indicate that Cu^{2+} binding to hIAPP can promote ROS generation, which is likely caused by the reduction of Cu^{2+} to Cu^{+} following the formation of the –O–Cu(aq)–N– ring structure.

3.1. Peptide backbone-Cu ring structure and the modulation of hIAPP aggregation

We explored the effects of the backbone-Cu^{2+} binding on hIAPP aggregation using thioflavin T (ThT) fluorescence and atomic force microscopy (AFM) measurements. An increase in ThT fluorescence signal (Fig. 4(a)) was observed upon incubation of hIAPP alone (as a control) for approximately 200 min, meaning the formation of fibrils. In the presence of Zn^{2+} (hIAPP + Zn^{2+}), the hIAPP fluorescence intensity, lag time and elongation rate (Fig. 4) were comparable to those of hIAPP alone. These results indicate that Zn^{2+} plays a modest role in hIAPP aggregation. In contrast, incubation of hIAPP with $CuCl_2$ (hIAPP + Cu^{2+}) caused an obvious decrease in ThT fluorescence intensity compared with that of hIAPP alone. Moreover, the lag time significantly increased to 535 min (2.5-fold of the control, Fig. 4(b)), and the elongation rate was reduced to 0.0035 min^{-1} (only 60% of the control, Fig. 4(c)). A larger number of the oligomer-like structures were clearly observed in the hIAPP + Cu^{2+} sample compared with the hIAPP alone and hIAPP + Zn^{2+} samples (Figs. 4(d)–4(f)). We attribute the remarkable difference of hIAPP aggregations between incubated with Cu^{2+} and Zn^{2+} to the significantly different manners of these ions binding to the peptide backbone. Namely, Cu^{2+}, but not Zn^{2+}, can bind to the peptide backbone by forming a ring structure. Therefore, the results above strongly indicate that the backbone-Cu ring structure plays an important role in the Cu^{2+} modulation of hIAPP aggregation via inhibiting peptide fibrillation and promoting oligomerization.

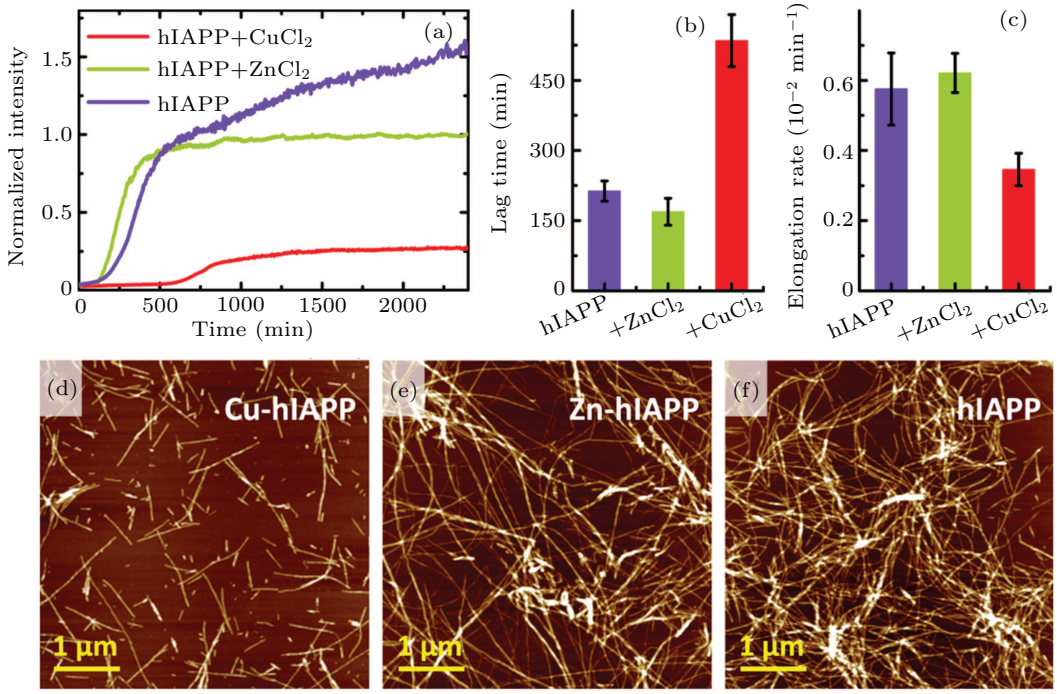


Fig. 4. Cu^{2+}-induced modulation of hIAPP aggregation. (a)–(c) ThT fluorescence intensity (a), lag time (b) and elongation rate (c) of hIAPP(1-37) in the absence and presence of $CuCl_2$, and $ZnCl_2$. (d)–(f) AFM images of hIAPP(1-37) in the presence of $CuCl_2$ (d), $ZnCl_2$ (e) and pure hIAPP(1-37) (f), following incubation for 3 days. A larger number of the oligomer-like structures clearly appear in the hIAPP + Cu^{2+} sample compared with the hIAPP alone and hIAPP + Zn^{2+} samples.

To further verify the relevance of the backbone-Cu binding model with the Cu^{2+}-induced modulation of IAPP aggregation, we also employed Li^{+} as a control, which has been used as a drug in clinic to slow the progress of amyloid-linked diseases.[29–31] The ThT fluorescence data (Figs. 5(a)–5(c)) showed that, compared with the case of only adding Cu^{2+}, the lag time of aggregation much significantly shortened in the case of pre-adding Li^{+} with five minutes in advance of adding Cu^{2+} (hIAPP + Li^{+} + Cu^{2+}, the ratio 1:5:5 of hIAPP, Li^{+} and Cu^{2+}), but the final intensity of fluorescence only weakly increased. These results indicate that the pre-addition of Li^{+} can remarkably decrease the effect of Cu^{2+} on the lag time

of aggregation, but play a weak role in the effect of Cu^{2+} on the final fluorescence intensity. Interestingly, in the case of only adding Li^+ (hIAPP + Li^+), the fluorescence intensity, lag time and elongation rate were comparable to those of hIAPP alone, denoting that Li^+ itself has negligible influence on the peptide aggregation. To explain these complicated and surprising phenomena, we calculated the binding energies of $Cu[(H_2O)_5]^{2+}$ and $[Li(H_2O)_4]^+$[32] with the carbonyl oxygen (–O–) on the Ser backbone (denoted as –O–*M*, $M = Cu(aq)^{2+}$ or $Li(aq)^+$) (Fig. 5(d)), respectively, as well as the binding energy of $Li(aq)^+$ upon forming a backbone ring structure (–O–Li(aq)–N–). The binding energies of –O–$Cu(aq)^{2+}$ and –O–$Li(aq)^+$ were −10.08 kcal/mol and −3.66 kcal/mol, respectively (Fig. 5(e)). Their difference was only 6.42 kcal/mol, very close to the hydrogen bond strength (∼ 5 kcal/mol) of water, indicating that Li^+ and Cu^{2+} can compete each other upon binding to the –O– in aqueous solution. The binding energy of $Li(aq)^+$ in the state –O–Li(aq)–N– was greater than +60 kcal/mol, strongly suggesting that Li^+ cannot form a backbone ring structure like Cu^{2+} does. Therefore, we can understand the above experimental observations as the following. The pre-added Li^+ can bind to the backbone –O–. The post-added Cu^{2+} will compete with the pre-added Li^+ to bind to the –O–. Due to the comparable binding strength between –O–$Li(aq)^+$ and –O–$Cu(aq)^{2+}$, this competition will take a long time, which results in the much significant difference of lag time between hIAPP + Li^+ + Cu^{2+} and hIAPP + Cu^{2+}. Additionally, Cu^{2+}, but not Li^+, can further replace the amide hydrogen H initially bound to –N– (Fig. 2(a)) to form a backbone ring structure –O–Cu(aq)–N–, reaching a more stable state (−27.65 kcal/mol). Thus the difference in the final intensity of ThT fluorescence between hIAPP + Li^+ + Cu^{2+} and hIAPP + Cu^{2+} is not so significant as the difference in lag time, while Li^+ itself cannot obviously affect the aggregation of hIAPP like Cu^{2+} does. Collectively, all of these results further strongly support that it is mainly through the backbone-Cu ring structure for Cu^{2+} to modulate the hIAPP aggregation.

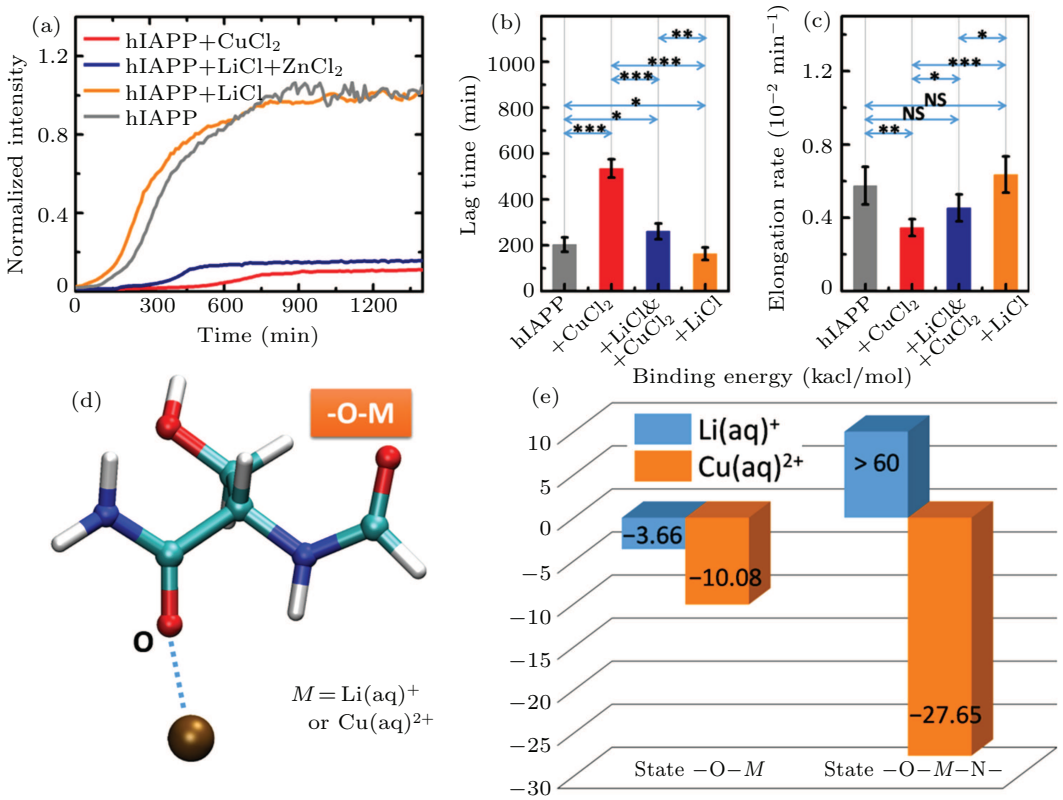


Fig. 5. Inhibitory effect of Li^+ on the Cu^{2+} modulation of hIAPP aggregation. (a)–(c) ThT fluorescence intensity (a), lag time (b) and elongation rate (c) of hIAPP(1-37) in the absence and presence of $CuCl_2$, LiCl, or both LiCl and $CuCl_2$. The concentration ratio of 1:1 is applied for $CuCl_2$ and LiCl. The label over the double-arrow line in the (b) and (c) panels indicates the two-tailed *P* value for statistically significant difference between the two groups of data: NS, *, **, and *** represent $P < 0.05$ (no significant difference), $P < 0.05$, $P < 0.01$, and $P < 0.001$, respectively. $N = 5$. (d)–(e) A theoretical model of Li^+ inhibiting the backbone-Cu ring formation. (d) A model peptide HCO-Ser-NH_2 for the state that a hydrated ion *M* (*M* = $Li(aq)^+$ or $Cu(aq)^{2+}$) binds to the carbonyl oxygen –O– of the peptide backbone, denoted as –O–*M*. The cyan, blue, red, white and brown spheres represent carbon, nitrogen, oxygen, hydrogen and copper, respectively. The dashed line indicates electrostatic attraction between the –O– and *M*. (e) Comparison of binding energies between the hydrated ions $Cu(aq)^{2+}$ and $Li(aq)^+$ in the states –O–*M* (left) and –O–*M*–N– (back-*M* ring structure, right), respectively. In the state –O–*M*, the difference of binding strength between $Cu(aq)^{2+}$ and $Li(aq)^+$ is only 6.42 kcal/mol, similar to the hydrogen bond strength (∼ 5 kcal/mol) of water, indicating that Li^+ can compete with Cu^{2+} upon binding to the –O– of backbone in aqueous solution. In the state –O–*M*–N–, the largely positive large value of binding energy for $Li(aq)^+$ strongly suggests that the Li^+ cannot form a backbone ring structure like Cu^{2+} does. Therefore, through the competition of the state –O–*M*, Li^+ can inhibit/delay the formation of backbone-Cu ring structure (the state –O–Cu(aq)–N–, Fig. 2(a)), although Li^+ itself is unable to form a backbone ring structure like Cu^{2+} does.

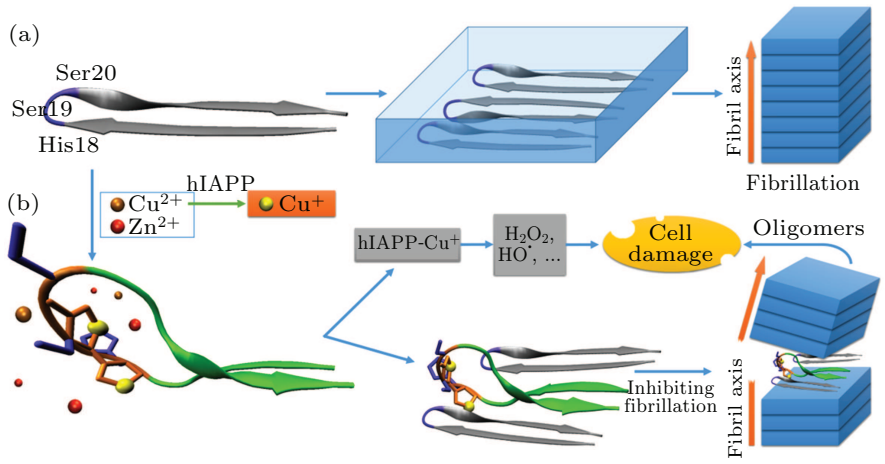


Fig. 6. A schematic representation for the molecular mechanism of Cu^{2+}-induced amyloid toxicity simultaneously involving both the enhancement of ROS level and the modulation of hIAPP aggregation. (a) Without the addition of Cu^{2+} or Zn^{2+}, the hIAPP peptide forms a β-sheet (middle, light blue block), as a molecular intermediate, stacking to cause hIAPP fibril formation (right, light blue column).[33] The silver ribbons represent the β strands, while the blue tube in between represents the turn region of His18−Ser20. (b) Due to the sidechain binding (supplementary Fig. 6), both Cu^{2+} (brown sphere) and Zn^{2+} (red sphere) ions can be enriched in the area close to the His18–Ser20 turn (blue sticks representing side chains). Cu^{2+} can bind to the backbones of His18, Ser19 (and/or Ser20) by forming a ring structure (orange sticks), which can be further stabilized by the His18 sidechain (Figs. 2(b) and 2(c)). This backbone binding reduces Cu^{2+} to Cu^{+} (yellow sphere), causing the formation of a hIAPP-Cu^{+} complex, which can largely enhance the ROS level in cells to damage the cells (oxidative stress hypothesis).[11,12] Additionally, the backbone-Cu^{+} ring structure substantially disrupts the β-sheet structure of peptides, dramatically inhibiting hIAPP fibrillation and promoting oligomerization. The oligomers will contribute more to cell damage than the fibrils (oligomer hypothesis).[14,15] In contrast to Cu^{2+}, Zn^{2+} cannot bind to the hIAPP backbone and is thus unable to induce the following effects on the ions and peptides as well as the consequent amyloid toxicity.

Finally, we explored the possible molecular mechanism of the Cu^{2+} modulation on hIAPP aggregation from the aspects of the backbone-Cu ring structure and the specific Cu^{2+} binding to the segment of His18, Ser19 and Ser20. We calculated the binding energies of $[Cu(H_2O)_5]^{2+}$ and $[Zn(H_2O)_6]^{2+}$ for the sidechains of His (through the coordination bond) and Ser (through the polar group). The binding strengths (supplementary Fig. 6) of Cu^{2+} and Zn^{2+} were comparable. The negative values of the binding energies indicate that these sidechains are able to bind/attract those cations. Therefore, the sidechains of His18−Ser20, particularly the His18 sidechain, can enrich both Cu^{2+} and Zn^{2+} in the local area (Fig. 6(b), left), which should largely promote the probability of ion backbone binding. However, as demonstrated above, only Cu^{2+} can stably form a ring structure with the peptide backbone. The stability of the backbone-Cu ring structure can be further enhanced by the His18 sidechain (Figs. 2(b) and 2(c)). This ring structure in the backbone will fix the dihedral angles between the two neighboring amide planes. Notably, Val17−Ser19 can form a turn structure that is critical for hIAPP fibrillation.[33] The backbone-Cu^{2+} binding in the His18−Ser20 segment should prevent or destroy this turn structure, thus inhibiting the formation of an intramolecular β-sheet structure (an intermediate molecular form for hIAPP assembly[33]). Additionally, the displacement of backbone amide protons (Figs. 1(b) and 2(a)) due to the backbone-Cu ring structure and the positive charge brought by Cu^{+} ion in the ring structure can further reduce the number of hydrogen bonds and the hydrophobicity of hIAPP peptides, respectively, which are the driving forces of fibril formation. All of these features will result in the inhibition of hIAPP fibrillation and the promotion of peptide oligomerization (Fig. 4(d)). Intriguingly, the binding energies of Zn^{2+} with the His18−Ser20 sidechains were comparable to those of Cu^{2+}. Thus, the lack of backbone binding is likely the primary reason for the modest effect of Zn^{2+} on the inhibition of hIAPP fibrillation (Fig. 4(e)).

4. Conclusion and perspectives

In summary, based on various biophysical approaches and theoretical analyses, we proposed a backbone-Cu^{2+} binding model at atomic resolution for the interaction between Cu^{2+} and amyloid peptide as well as the consequent effects (Fig. 6). Redox-active Cu^{2+} can bind to the hIAPP backbone by forming a ring structure, which caused the reduction of Cu^{2+} to Cu^{+} to enhance ROS levels in cells. Moreover, the backbone-Cu^{2+} binding also dramatically inhibited peptide fibrillation and promoted oligomerization. In contrast to Cu^{2+}, additional biologically important cations, such as Zn^{2+}, cannot bind to the backbone and thus do not induce the subsequent effects. Furthermore, we also found that Li^{+} considerably weakened the effects of Cu^{2+} on hIAPP, which suggests a clue for inhibiting copper-mediated amyloid toxicity through blocking or destroying the backbone-Cu ring structure. These findings thus provide a new molecular mechanism simultaneously for Cu^{2+}-induced ROS generation and hIAPP aggregation which are significantly involved in amyloid toxicity, potentially promoting the understanding of Cu-mediated amyloid toxicity at atomic resolution, and even the development of drug design and therapy for type-2 diabetes and other diseases.

5. Methods

Nuclear magnetic resonance spectroscopy The hIAPP(11-28) peptide was dissolved in ice-cold water to get a stock solution with the peptide concentration of 0.15 mM. This stock solution was stored at −80 °C. To prepare the NMR sample, the stock peptide solution was dissolved in 10 mM sodium phosphate buffer (pH 4.3) to make the peptide concentration to be 0.12 mM.

All NMR experiments were performed at 283 K on a Bruker AVANCE spectrometer operating at 600 MHz (proton frequency) and equipped with a 5 mm, pulsed-field gradient triple-resonance probe. Two-dimensional (2D) ^{1}H–^{1}H total correlation spectroscopy (TOCSY) spectra were acquired with a mixing time of 80 ms using the MLEV-17 spin-lock sequence to drive the coherence transfer. 2D ^{1}H–^{1}H nuclear Overhauser effect spectroscopy (NOESY) spectra were obtained using the mixing time of 400 ms. All 2D spectra were acquired in the phase-sensitive mode. To reduce the water peak in 2D spectra, WATERGATE suppression was used. The ^{1}H resonance spin systems were assigned from the analysis of TOCSY spectra. Sequential assignments were made from the sequential connectivity information of d_{NN} and $d_{\alpha N}$ in the NOESY spectra.

NMR titration experiments were carried out by adding $CuCl_2$ or $ZnCl_2$ to 0.12 mM hIAPP(11-28) peptide dissolved in 10 mM sodium phosphate buffer (pH 4.3C). TOCSY spectra were measured at the Cu^{2+} or Zn^{2+} concentration of 0 mM and 0.60 mM, respectively. Peak intensities were compared for the two TOCSY spectra at the Cu^{2+} or Zn^{2+} concentration of 0 mM and 0.60 mM, respectively.

X-ray absorption fine structure spectra XAFS measurements (including EXAFS and XANES) were collected at Shanghai Synchrotron Radiation Facility (SSRF) beamline BL14W. A Si[111] double crystal monochromator and a set of focusing mirrors with a cut-off energy of 22.5 keV were used throughout the study. The XAFS spectra were recorded in fluorescence mode using a 32-element Ge solid-state detector. Data collected in each run were first averaged and after background subtraction, the resulting spectra were normalized. To prepare a sample for XAFS measurement, 1500 ml 20 μM hIAPP (hIAPP(1-37), hIAPP(1-11), hIAPP(11-28) and hIAPP(28-37), respectively) peptide with and without 200 μM $ZnCl_2$ or 200 μM $CuCl_2$ at pH 4.5 was incubated at 37 °C for three days, respectively. In order to increase the signal/noise ratio in XAFS data, each of these samples were further concentrated to 300 ml by freeze drying.

DCFH-DA fluorescence Intracellular ROS amount was measured by ROS-sensitive probe DCFH-DA. INS-1 cells seeded in 6-well microplates at a concentration of 5×10^4 cells/ml were cultured at 37 °C in a humidified atmosphere for 48 h. Then the cell was incubated with hIAPP(1-37) (as a control, 20 μM), 100 μM $CuCl_2$, or co-incubated with both 20 μM hIAPP and 100 μM $CuCl_2$ for 48 h. After that, the cells were loaded with DCFH-DA at a final concentration of 10 μM at 37 °C for 60 min. The cells were washed with 10 mM PBS and then transferred to a 96-well plate. ROS generation was assessed by measuring the fluorescence intensity with a microplate reader (Thermo Scientific Fluoroskan Ascent FL) at the excitation and emission wavelengthes of 485 nm and 525 nm, respectively.

ThT fluorescence The kinetics of hIAPP(1-37) fibril formation was detected by fluorescence intensity increase upon binding of the fluorescent dye ThT to fibrils. To prepare a sample for fluorescence, the hIAPP(1-37) peptide was diluted to a final concentration of 20 μM using sodium phosphate buffer containing 20 μM ThT and 200 μM $ZnCl_2$, $CuCl_2$, or LiCl at pH 4.5. The pH of each sample was individually adjusted. Fluorescence was measured using a luminescence spectrometer (Thermo Scientific Fluoroskan Ascent FL) in a sealed Corning 96 well at 37 °C. The excitation and emission wavelength was 440 nm and 485 nm, respectively. A common sigmoidal growth model was used to fit the time-dependent ThT fluorescence curves to extract lag time and elongation rate constants.[34]

AFM measurement 20 μM hIAPP(1-37) peptide with and without 200 μM $ZnCl_2$ or 200 μM $CuCl_2$ at pH 4.5 was incubated at 37 °C for three days, respectively. Then a 5 μl incubated solution was deposited onto a freshly cleaved mica, waited for 5 min, gently rinsed with Milli-Q water and dried in air. Images were collected using a Multimode 8 with Controller V scanning force microscope (Bruker) operated in tapping mode in air. Images were simply flattened using the NanoScope analysis software.

Simulations and calculations All of simulations and calculations were performed using an *ab initio* method based on the second order Møller–Plesset perturbation theory (MP2),[35] as implemented in the Gaussian09 package with the 6-31+G(d,p) basis set and including diffuse functions was applied on all atoms.

To calculate the backbone binding energy of hydrated M ion $[M(H_2O)_n]_{2+}$ (M = Cu, Zn, Mg, Ca) on the backbone of model peptide HCO-Ser-NH_2 ($C_4N_2O_3H_8$) in Fig. 2(a), we applied the following formula:

$$E_{\text{binding}} = E\left(C_4N_2O_3H_7\cdot\left[M\left(H_2O\right)_{n-2}\right]^+\right) + E\left(H_2O\right) - E\left(C_4N_2O_3H_8\right) - E\left(\left[M\left(H_2O\right)_n\right]^{2+}\right), \quad (1)$$

where the first, second, third and fourth terms in the right side of equation indicate the energy of the backbone ring structure, molecules H_2O and H_3O^+, peptide HCO-Ser-NH_2, and hydrated M ion $[M(H_2O)_n]^{2+}$, respectively. The index $n = 5$ for M = Cu, and $n = 6$ for M = Zn, Mg and Ca.

To calculate the binding energy of the backbone-Cu ring structure and His sidechain in Fig. 2(b), we applied the following formula:

$$E_{\text{binding}} = E\left(\text{Sidechain}\cdot[\text{BackboneRing}]^{+}\right) + E\left(H_2O\right) - E\left([\text{BackboneRing}]^{+}\right) - E\left(\text{Sidechain}\right), \quad (2)$$

where the first, second, third, and fourth terms in the right side of equation stand for the energies of the complex of His sidechain and backbone-Cu ring, water molecule H_2O, backbone-Cu ring, and His sidechain, respectively.

Acknowledgements

We thank Prof. Jun Hu and Prof. Bo Song for discussions. All the calculations were performed on the Shanghai Supercomputer Center of China. Figure 3(a) was reproduced from Ref. [25] with permission from the Royal Society of Chemistry.

Project supported by the National Natural Science Foundation of China (Grant Nos. 12074208 and 11375256), the Natural Science Foundation of Jiangsu Province (Grant No. BK20200176), the Natural Science Foundation of Jiangsu Higher Education Institutions of China (Grant Nos. 20KJB140020 and 19KJB140005), Fundamental Research Project from Changzhou Science and Technology (Grant No. CJ20200029), and the Jiangsu Province High-level Innovative and Entrepreneurial Talents Introduction Plan.

References

[1] Kim B E, Nevitt T and Thiele D J 2008 *Nat. Chem. Biol.* **4** 176
[2] Faller P, Hureau C and Penna La G 2014 *Acc. Chem. Res.* **47** 2252
[3] Kim D, Bang J K and Kim S H 2015 *Angew. Chem. Int. Ed.* **54** 1561
[4] Branch T, Girvan P, Barahona M and Ying L 2015 *Angew. Chem. Int. Ed.* **54** 1227
[5] Liu Y, Nguyen M, Robert A and Meunier B 2019 *Acc. Chem. Res.* **52** 2026
[6] Lu T, Aron L, Zullo J, Pan Y, Kim H, Chen Y, Yang T H, Kim Y M, Drake D, Liu X S, Bennett D A, Colaiácovo M P and Yankner B A 2014 *Nature* **507** 448
[7] Atrián-Blasco E, Gonzalez P, Santoro A, Alies B, Faller P and Hureau C 2018 *Coordin. Chem. Rev.* **371** 38
[8] Smith D P, Ciccotosto G D, Tew D J, Fodero-Tavoletti M T, Johanssen T, Masters C L, Barnham K J and Cappai R 2007 *Biochemistry* **46** 2881
[9] Bozkurt F, Tekin R, Gulsun S, SatıcıÖ, Deveci O and Hosoglu S 2013 *Int. J. Diabetes Dev. Ctries.* **33** 165
[10] Zatta P, Drago D, Bolognin S and Sensi S L 2009 *Trends Pharmacol Sci.* **30** 346
[11] Barnham K J, Masters C L and Bush A I 2004 *Nat. Rev. Drug Discov.* **3** 205
[12] Cassagnes L E, Herv V, Nepveu F, Hureau C, Faller P and Collin F 2013 *Angew. Chem. Int. Ed.* **52** 11110
[13] Himes R A, Park G P, Siluvai G S, Blackburn N J and Karlin K D 2008 *Angew. Chem. Int. Ed.* **47** 9084
[14] Hardy J and Selkoe D J 2002 *Science* **297** 353
[15] Kayed R, Head E, Thompson J L, McIntire T M, Milton S C, Cotman C W and Glabe C G 2003 *Science* **300** 486
[16] Yu Y P, Lei P, Hu J, Wu W H, Zhao Y F and Li Y M 2010 *Chem. Commun.* **46** 6909
[17] Dong X, Svantesson T, Sholts S B, Wallin C, Jarvet J, Graslund A and Wärmländer S K T S 2019 *Biochem. Biophys. Res. Commun.* **510** 520
[18] Mold M, Ouro-Gnao L, Wieckowski B M and Exley E 2013 *Sci. Rep.* **3** 1256
[19] Stefaniak E, Atrian-Blasco E, Goch W, Sabater L, Hureau C and Bal W 2021 *Chem. Eur. J.* **27** 2798
[20] Poulson B G, Szczepski K, Lachowicz J I, Jaremko L, Emwas A H and Jaremko M 2020 *RSC Adv.* **10** 215
[21] Yang T, Yu T, Zhao W and Lin D 2021 *Chin. Phys. B* **30** 088701
[22] Lorenzo A, Razzaboni B, Weir G and Yankner B 1994 *Nature* **368** 756
[23] Mazor Y, Gilead S, Benhar I and Gazit E 2002 *J. Mol. Biol.* **322** 1013
[24] Pasquarello A, Petri I, Salmon P S, Parisel O, Car R, Tóthé, Powell D H, Fischer H E, Helm L and Merbach A E 2001 *Science* **291** 856
[25] Rudolph W W and Pye C C 1999 *Phys. Chem. Chem. Phys.* **1** 4583
[26] Huo G, Chen W, Wang J, Chu X, Xu W, Li B, Zhang Y, Xu B and Zhou X 2020 *RSC Adv.* **10** 5566
[27] Song B, Sun Q, Li H, Ge B, Pan J S, Wee A T S, Zhang Y, Huang S, Zhou R, Gao X, Huang F and Fang H 2014 *Angew. Chem. Int. Ed.* **53** 6358
[28] Lincoln K M, Richardson T E, Rutter L, Gonzalez P, Simpkins J W and Green K N 2012 *ACS Chem. Neurosci.* **3** 919
[29] Forlenza O V, De-Paula V J R and Diniz B S O 2014 *ACS Chem. Neurosci.* **5** 443
[30] Chiu C T and Chuang D M 2010 *Pharmacol. Therapeut.* **128** 281
[31] Forlenza O V, Radanovic M, Talib L and Gattaz W 2019 *Br. J. Psychiatry.* **215** 668
[32] Varma S and Rempe S B 2006 *Biophys. Chem.* **124** 192
[33] Jaikaran E T A S and Clark A 2001 *Biochimica et Biophysica Acta* **1537** 179
[34] Brender J R, Hartman K, Nanga R P, Popovych N, Salud Bea de la R, Vivekanandan S, Marsh E N and Ramamoorthy A 2010 *J. Am. Chem. Soc.* **132** 8973
[35] Møller C and Plesset M S 1934 *Phys. Rev.* **46** 618